THIN GRANULAR LAYER ON A VIBRATING PLATE. SWIFT–HOHENBERG EQUATION

Mircea Bogdan TATARU
University of Oradea, btataru@uoradea.ro

Key words: ,labyrinthine, decorated interfaces, superoscillons, subharmonic drivi ng

Abstract: An experimental study of patterns in vibrated granular layers is presented. Swift-Hohenberg equation (SHE) obtained from Ginzburg-Landau equation by rescaling, gives the opportunity to discuss control on interface motion and object dynamics. Experiments confirm existence of superoscillons and bound states of superoscillons and interfaces. On the basis of the order parameter model it is predicted theoretically and confirmed experimentally that additional subharmonic driving results in the controlled motion of interfaces.

1. Introduction

Driving control possibilities of a thin granular layer on a vibrating plate gives the technical opportunity to build a special kind of separating devices which use this kind of behavior in granular material separation on vibrating surfaces like sieves or hole-plates.

In this paper is demonstrated that in a certain limit model can be reduced to the real Swift-Hohenberg equation. This equation also possesses a similar variety of patterns including stripes, hexagons, stable and unstable interface solutions, and localized solutions. In section 3 is demonstrated that additional subharmonic driving results in drift of the interface with the velocity determined by the amplitude of the driving and the direction determined by the relative phase. In section 4 experimental results are presented. This includes a phase diagram and the effect of additional sub-harmonic driving. Section 5 summarizes conclusions.

2. Swift-Hohenberg equation

Near the line $s=1$ (see Fig. 7 from previous paper) equation (3) can be simplified. In the vicinity of this line $A\sim(s-1)^{1/2}$ and $B\sim(s-1)^{3/2}<<A$. In leading order we can obtain $B=b.\nabla^2 A/2$ from equation (5), and equation (4) yields [1]:

$$\partial_t A=(s-1).A-A^3+(1-w.b).\nabla^2 A-\frac{b^2}{2}\cdot\nabla^4 A \tag{1}$$

Rescaling the variables, $t\to(s-1).t$, $A\to(s-1)^{-1/2}.A$, $x\to\left[2(s-1)/b^2\right]^{1/4}$, we arrive at the Swift-Hohenberg equation (SHE):

$$\partial_t A=A-A^3-d\nabla^2 A-\nabla^4 A \tag{2}$$

where:

$$d=\frac{w.b-1}{b}\cdot\sqrt{\frac{2}{s-1}} \tag{3}$$

The description by the SHE. is valid if, $d\sim O(1)$, which implies an additional condition for the validity of his approach $w.b-1<<1$ at $s\to 1$.

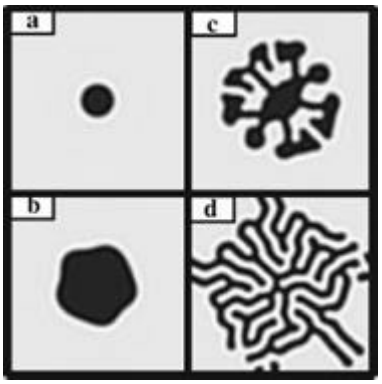

Fig. 1. (a)–(d) Labyrinth formation from a circular spot (SHE); $d=1{,}4$, the domain size is 100×100 units, and $t=200,\ 1300,\ 1700,\ 1900$

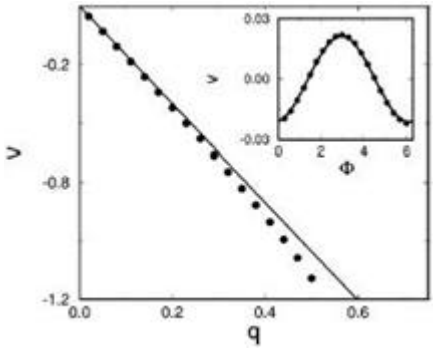

Fig. 2. Interface velocity u for $w=1$, $b=4$, and $g=2{,}5$ vs q at $\Phi=0$. Inset: u vs. Φ at $q=0{,}01$. (●), numerical results; (—), analytical expression (30)

Although this equation is simpler than equation (3), it captures many essential features of the original system dynamics, including the existence and stability of stripes and hexagons in different parameter regions (see references [2, 3]); the existence of the interface solutions, interface instability, and superoscillons; and the emergence of labyrinthine patterns [3]. Indeed, a simple analysis shows that the growth rate of the instability of the uniform state $A=1$ as a function of the perturbation wave number is determined by the formula $l(k)=-2+d.k^2-k^4$; it becomes unstable at $d>d_C=2\sqrt{2}$ a critical wave number $k_C=\sqrt{2}$. As in the original model, near the threshold of this instability, subcritical hexagonal patterns are preferred. The interface stability can also be analyzed more simply, as the linearized operator corresponding to model (2) is self-adjoint. The threshold value of d is obtained from the solvability condition:

$$\int_{-\infty}^{\infty}\left(d_{th}.A_{0x}^2-2A_{0x}^2\right)\cdot dx=0 \tag{4}$$

which yields $d_{th}=1{,}011$. This yields an equation for the neutral curve of the interface instability in the Swift-Hohenberg limit in the form:

$$s=1+\frac{2(w.b-1)^2}{d_{th}^2.b^2} \tag{5}$$

Figures 1(a)–1(d) show the development of the interface instability within the SHE with a subsequent transition to labyrinthine patterns, similar to the dynamics of the full parametric equation (3). Again, to saturate the instability, an additional non-local mechanism is required.

As was shown recently, the Swift-Hohenberg equation also possesses localized solutions (see references [3, 4]). These localized states are analogous to the superoscillons of equations (3).

3. Sub-harmonic forcing and interface motion

Now we will focus on the effect of additional subharmonic driving on the motion of the interface. In the original model equation (3) from [ ], the interface does not move due to symmetry between the left and right halves of the interface. However, if the plate oscillates

with two frequencies f and $f/2$, the symmetry between these two states, connected by the interface, is broken, and the interface moves. The velocity of the interface motion depends on the relative phase of the subharmonic forcing with respect to the forcing at f. The effect of a small external subharmonic driving applied in the background of the primary harmonic driving with the frequency f can be described by the equation cf. equation (3) previous paper:

$$\partial_t y = g.y^* - (1-iw).y + (1+ib).\nabla^2 y - |y|^2 y + qe^{i\Phi} \tag{6}$$

where q characterizes the amplitude of the subharmonic pumping, and Φ determines its relative phase.

For small, q we look for a moving interface solution in the forms $y = y_0(x-u.t) + q.y_1(x-u.t) + \ldots$ and $u = O(q)$, or, alternatively,

$$\begin{pmatrix} A \\ B \end{pmatrix} = \begin{pmatrix} A_0(x-u.t) \\ B_0(x-u.t) \end{pmatrix} + q\begin{pmatrix} a(x-u.t) \\ b(x-u.t) \end{pmatrix} + O(q^2) \tag{7}$$

The solvability condition compare with equation (21) previous paper fixes the interface velocity as a function of the amplitude and phase of the external subharmonic driving:

$$u = -q \cdot \frac{\cos\Phi.\int A^\dagger dx + \sin\Phi.\int B^\dagger dx}{\cos\Phi.\int \left(A^\dagger \partial_x A_0 + B^\dagger \partial_x B_0\right).dx} = q.a.\sin(\Phi - \Phi_0) \tag{8}$$

where $a = \text{const.}$ is the susceptibility of the interface for external forcing, and $\Phi_0 = \text{const.}$ is some phase shift. An explicit answer is obtained for $b = 0$ when $A^\dagger = \partial_x.A_0$ and $\mathrm{F} = 0,p$, which yields the interface velocity $u = \mp\frac{3}{2}\cdot qA_0^{-2} = \mp\frac{3}{2}\cdot q\cdot(s-1)^{-1}$. In general, $A,$, B, $A^\dagger$, and $B^\dagger$, and hence u, can be found numerically. The interface velocity as function of q,Φ is shown in Fig. 2.

Thus from this analysis we conclude that additional subharmonic driving results in a controlled motion of the interface. The velocity of the interface depends on the amplitude of the driving, and the direction is determined by the relative phase Φ.

4. Experimental results

There were performed experiments with a thin layer of granular material subjected to periodic driving. The experimental setup is similar to that of reference [6]. Were used 0.15 mm diameter bronze or copper balls, and the layer thickness in our experiments was ten particles.

Experiments were performed in a rectangular cell of, $4\times12\ \mathrm{cm}^2$ with possibility to vary the acceleration Γ and frequency f of the primary driving signal as well as the acceleration g, frequency f_1 and phase Φ of the secondary (additional) driving signal.

The interface position and vertical accelerations were acquired using high-speed

video and accelerometers, and further analyzed on a computer. To maintain and measure the proper acceleration at f and $f/2$ we employed the lock-in technique with our signal

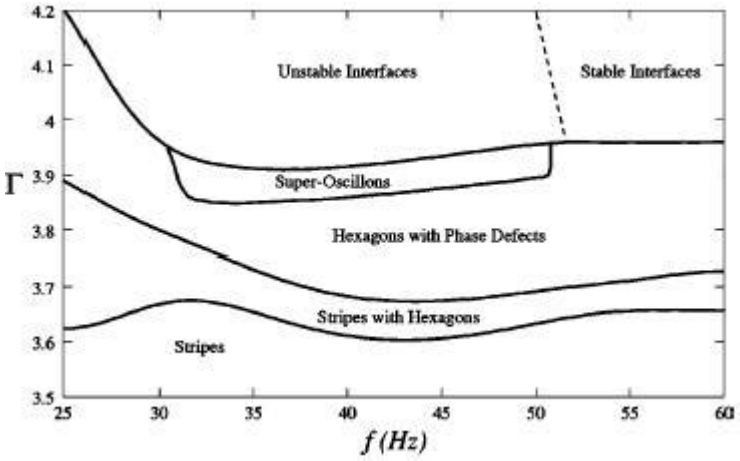

Fig. 3. Phase diagram. The material is $150\,\mu m$ ***copper balls, and the layer thickness is ten time particle diameters***

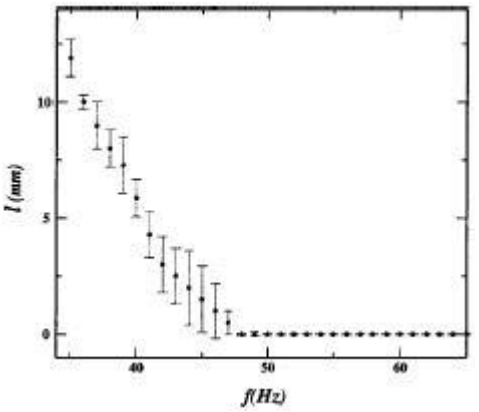

Fig. 4. The amplitude of periodic undulations l ***as a function of driving frequency*** f ***. The acceleration amplitude is*** $\Gamma = 4{,}1$.

originating from an accelerometer attached to the bottom of the cell. This allowed for simultaneous real-time feedback and control of the device. To reduce the interstitial gas effects [5] we reduced the pressure to $2\,\mathrm{mTorr}$. Our visual data were acquired using a high-speed digital camera (Kodak SR-1000c), in addition to high-speed recording this also allowed for a synchronization between the patterns and the image acquisition.

4.1. Phase diagram

The experimental phase diagram is shown in Fig. 3.,The transition from hexagons to interfaces is elaborated in more detail. There is a small hysteresis at the transition line from stripes to hexagons (not shown in the phase diagram). The dashed line indicates the stability line for interfaces with respect to periodic undulations, determined as the average half-width of the pattern. To determine this stability limit, we kept the value of acceleration Γ fixed and increased the driving frequency, f. For each value of the frequency the interface width was extracted by averaging up to ten images of the interface. In order to find that amplitude of the periodic undulations l the thickness of the flat interface l_0 was subtracted from the obtained value. The resultant amplitude or undulations l as functions of driving frequency f are shown in Fig. 4. As one sees from the figure, the amplitude of undulations l decreases gradually, approaching the critical value of the frequency. However, a small hysteresis at the transition point cannot be excluded because of large error bars.

As follows from the phase diagram, for a small amplitude of the vertical acceleration $\Gamma < 3{,}6$ stripes are the only stable pattern. At slightly higher values ($\Gamma = 3{,}6...3{,}7$) stripes and hexagons coexist. For higher values ($\Gamma = 3{,}7...4{,}0$) the hexagons become stable. Due to the sub-harmonic character of motion both up and down hexagons may coexist, separated by a line phase defect (Fig. 5.a.). There exists a narrow band, from $\Gamma = 3{,}85...4{,}0$, where localized states, or superoscillons, appear both within the bulk of the material and also pinned to the front between the interface and the bulk (Fig. 5.b.). For even higher values of the acceleration $\Gamma > 4{,}0$ the superoscillons disappear (Fig. 5.c.), leading to isolated interfaces with periodic decorations.

4.2. Controlled motion of interface

In the absence of additional driving the interface drifts toward the middle of the cell (see Fig. 5). We attribute this effect to the feedback between the oscillating granular layer and the plate vibrations, due to the finite ratio of the mass of the granular material to the mass of the vibrating plate. Even in the absence of sub-harmonic drive, the vibrating cell can acquire sub-harmonic motion from the periodic impacts of the granular layer on the bottom plate at half the driving frequency.

If the interface is located in the middle of the cell, the masses of material on both sides of the interface are equal, and, due to the anti-phase character of the layer motion on both sides, an additional sub-harmonic driving is not produced. The displacement of the interface X from the center of the cell leads to a mass difference Δm on opposite sides of the interface, which in turn causes an additional sub harmonic driving proportional to Δm. In a rectangular cell, $\Delta m \propto X$. Our experiments show that the interface moves in such a way to decrease the sub-harmonic response, and the feedback provides an additional term $-X/t$ on the right-hand side of equation (8), yielding

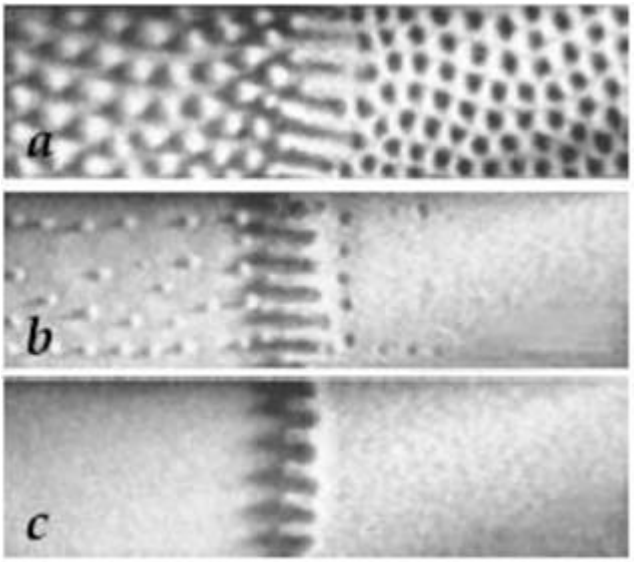

Fig. 5. Representative high-acceleration patterns in the rectangular $4\times12\ \mathrm{cm}^2$ ***cell, driving frequency*** $f = 40\ \mathrm{Hz}$***: (a)*** $\Gamma = 3{,}75$ ***shows the onset of the interface with up and down hexagons. (b)*** $\Gamma = 3{,}94$ ***supe-oscillons are present in the flat layer and are pinned to the front near the interface. (c)*** $\Gamma = 4$***, isolated decorated interface.***

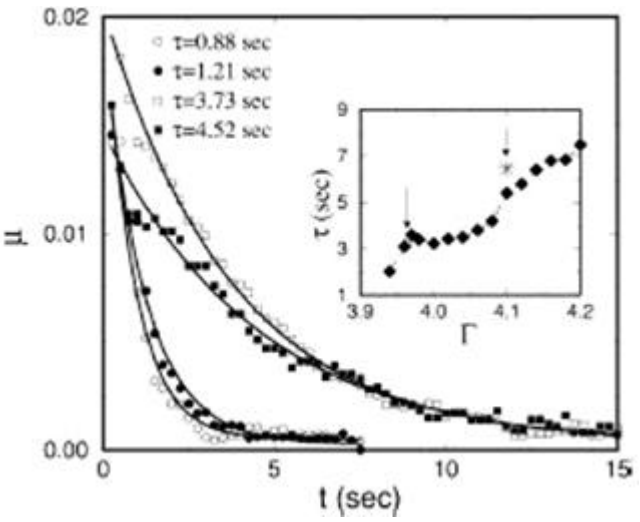

Fig. 6. Amplitude of the sub-harmonic acceleration m ***of the cell averaged over four measurements vs. time for the interface propagating to the center of the cell for*** $\Gamma = 3{,}97$ ***and*** $f = 40\ \mathrm{Hz}$***. Circles and squares correspond to circular and rectangular cells, and open and closed symbols correspond to light and heavy cells, respectively. Heavy cells differ from light ones by an additional weight of 250 g attached to the moving shaft. Solid lines show an exponential fit*** $m \sim \exp(t/t) + \mathrm{const.}$ ***.Inset:*** t ***vs*** Γ ***for light rectangular cell.***

$$\frac{dX}{dt} = -X/t + qa.\sin(\Phi - \Phi_0) \tag{9}$$

The relaxation time constant t depends on the mass ratio (this also holds for the circular cell if X is small compared to the cell radius). Thus, in the absence of an

additional sub-harmonic drive ($q = 0$), the interface will eventually divide the cell into two regions of equal area (see Fig. 5).

In order to verify the prediction of equation (9) the following experiment was performed: The interface was positioned off center by applying an additional subharmonic drive. Then we turned off the subharmonic drive and immediately measured the amplitude m of the plate acceleration at the sub-harmonic frequency [5]. The results are presented in Fig. 6. The subharmonic acceleration of the cell decreases exponentially as the interface propagates to the center of the cell. The measured relaxation time t of the subharmonic acceleration increases with the mass ratio of the granular layer and of the cell with all other parameters fixed. The mass of the granular layer was varied by using two different cell sizes - circular, diameter 153 mm, and rectangular, 40x120 mm^2 - while keeping the thickness of the layer unchanged. For these cells we found that the relaxation time t in the rectangular cell is about four times greater than for the circular cell (see Fig. 6). This is consistent with the ratio of the total masses of granular material (52 grams in rectangular cell and 198 grams in the circular cell). In a separate experiment the mass of the cell was changed by attaching an additional weight of 250 grams to the moving shaft, which weighs 2300 grams. This led to an increase of the corresponding relaxation times of 15–25%. The relaxation time t increases rapidly with Γ (see the inset of Fig. 6).

When an additional subharmonic driving is applied, the interface is displaced from the middle of the cell. For small amplitude of the subharmonic driving g, the stationary interface position is $X = qa.\sin(\Phi - \Phi_0)$, since the restoring force balances the external driving force. The equilibrium position X as function of Φ is shown in Fig. 7.a. The solid line depicts the sinusoidal fit predicted by the theory. Because of the finite mass ratio effect, the amplitude of the measured plate acceleration m at frequency f_1 also shows periodic behavior with Φ (see Fig. 7.b), enabling us to infer the interface displacement from the acceleration measurements.

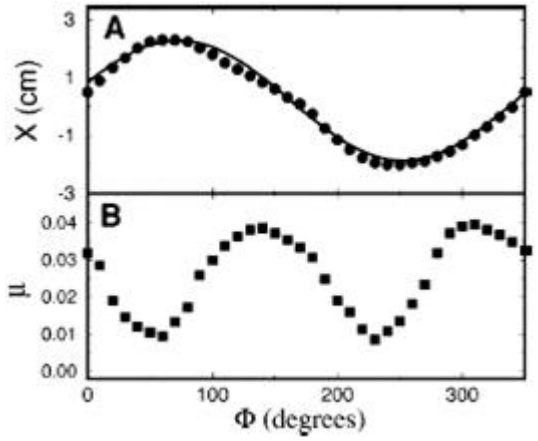

Fig. 7. (a) Equilibrium position X and (b) amplitude of measured sub-harmonic acceleration m as functions of phase Φ. Circular cell: $\Gamma = 4{,}1$ and $f = 40$ Hz, and $q = 1{,}25\%$ of Γ.

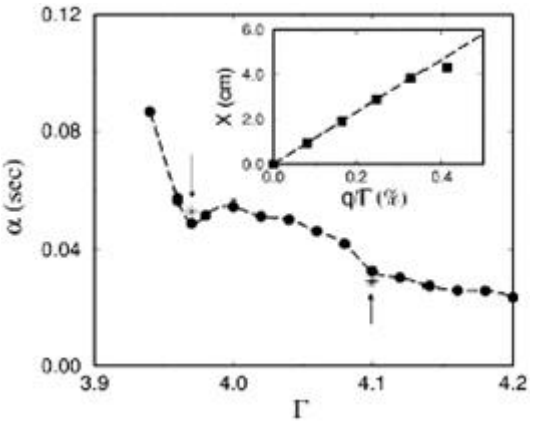

Fig. 8. Susceptibility α vs. Γ at $f = 40$ Hz, rectangular cell. Inset: displacement X as a function of q at $\Phi = 260°$.

For an even larger amplitude of sub-harmonic driving (more than 4–5% of the primary driving) extended patterns (hexagons) re-emerge throughout the cell.

The velocity $V_0 = qa$, which the interface would have in an infinite system, can be found from measurements of the relaxation time t and maximum displacement X_m at a given amplitude of subharmonic acceleration g, $V_0 = X_m / t$; see equation (9). We verified

that in the rectangular cell the displacement X depends linearly on g almost up to values at which the interface disappears at the short side wall of the cell (see the inset of Fig. 8). Figure 8 shows the susceptibility a as a function of the amplitude of the primary acceleration Γ. The susceptibility decreases with Γ. The cusp-like features in the Γ dependence of a (and t; see the inset to Fig. 6) are presumably related to the commensurability between the lateral size of the cell and the wavelength of the interface decorations.

We developed an alternative experimental technique which allowed us to measure simultaneously the relaxation time t and the ''asymptotic'' velocity V_0. This was achieved by a small detuning Δf of the additional frequency f_1 from the exact sub-harmonic frequency $f/2$, i.e., $\Delta f = f_1 - f/2 << f$. This is equivalent to the linear increase of the phase shift Φ with the rate $2p.\Delta f$. This linear growth of the phase results in a periodic motion of the interface with frequency Δf and amplitude $X_m = V_0 / \sqrt{t^{-2} + (2p.\Delta f)^2}$ (see equation (9)). The measurements of the ''response functions'' $X_m(\Delta f)$ are presented in Fig. 16. From the dependence of X_m on Δf we can extract parameters V_0, a, and t by a fit to the theoretical function. The measurements are in a very good agreement with previous independent measurements of the relaxation time t and susceptibility a. For a comparison with the previous results, we indicate the values for t and a, obtained from the response function measurements of Fig. 6 and Fig. 8 (stars). The measurements agree within 5%.

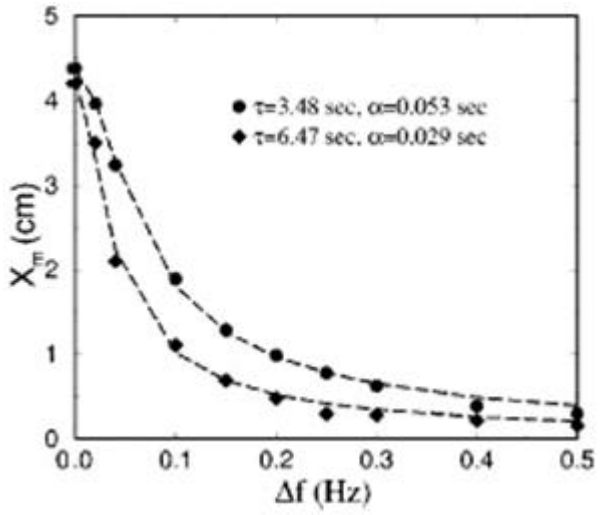

Fig. 9. Maximum displacement X_m from the center of the rectangular cell as a function of frequency difference $\Delta f = f_1 - f/2$ for $f = 40$ Hz, and for $\Gamma = 3{,}97$ (circles) and $\Gamma = 4{,}1$ (diamonds). Dashed lines are fit to $X_m = V_0 / \sqrt{t^{-2} + (2p.\Delta f)^2}$. The values of a and t obtained from the fit are also indicated in Figs. 13 and 15 by arrows with stars.

5. Conclusions

Interface decorations were found to be a result of the transversal instability of a flat interface, which is analogous to the negative surface tension. We found that equation (3) in the previous theory is not sufficient to describe the saturation of the interface instability. We propose a possible non-local mechanism of saturation of this instability which takes into account the dependence of the overall length of the interface and the magnitude of parametric forcing, which may occur due to a large scale convective flow induced by the sand motion near the interface. We described analytically the motion of the interface under the symmetry-breaking influence of the small sub-harmonic driving. In our experimental study we found that on a qualitative level the theoretical phase diagram is similar to the experimental one. The experiments also confirmed the existence of superoscillons and their bound states with the interface, as predicted by the theory. Further experimental study is necessary to elucidate the specific mechanism for saturation of the interface instability.

Stimulated by the theoretical prediction, we also performed experimental studies of interface motion under additional sub-harmonic driving. The experiment confirmed that the direction and magnitude of the interface displacement depend sensitively on the amplitude and relative phase of the sub-harmonic driving. Moreover, we found that the period-doubling motion of the flat layers produces sub-harmonic driving because of the finite ratio of the mass of the granular layer and the cell. This in turn leads to the restoring force driving the interface toward the middle of the cell.

References

1. Coullet P., and K. Emilson SHE for oscillatory systems with strong resonance coupling was derived by, Physica D 61, 119 **(1992)**.
2. Dewel, G., S. Métens, M'F. Hilali, P. Borckmans, and C.B. Price, Phys. Rev. Lett. 74, 4647 **(1995)**.
3. Aranson, I. S., B. A. Malomed, L. M. Pismen, and L. S. Tsimring (unpublished).
4. Ouchi K., and H. Fujisaka, Phys. Rev. E 54, 3895 **(1996)**; K. Staliunas and V.J. Sánchez-Morcillo, Phys. Lett. A 241, 28 **(1998)**.
5. Pak, H.K., E. VanDoorn, and R.P. Behringer, Phys. Rev. Lett. 74, 4643 **(1995).**

***) Papers are referenced in apparition order**